Catalysis Science & Technology

Accepted Manuscript

ROYAL SOCIETY OF CHEMISTRY

www.rsc.org/catalysis

Journal Name

ARTICLE

A new insight into morphology effect of ceria on CuO/CeO_2 catalysts for CO selective oxidation in hydrogen-rich gas

Xiaolin Guo[a] and Renxian Zhou*[a]

Received 00th January 20xx,
Accepted 00th January 20xx

DOI: 10.1039/x0xx00000x

www.rsc.org/

We prepared four ceria supports with different morphologies (rod, cube, plate and polyhedra) by hydrothermal methods and supported copper oxide catalysts, which is used for selective oxidation of CO in hydrogen-rich gas and characterized by various techniques. The results show that CuO/CeO_2-rod and CuO/CeO_2-polyhedra exhibit higher low-temperature catalytic oxidation activity coupled with broader operating temperature "window" (CO conversion > 99.0 %, 95-125 °C and 90-125 °C, respectively) in CO selective oxidation reaction, due to higher content of the active species Cu^+, the smaller copper oxide clusters subjected to a strong interaction with ceria and more oxygen vacancies on the surface of the catalysts. In addition, higher specific surface area, smaller average pore size and concentrated pore-size distribution of mesopores are also beneficial to improving the catalytic performance. However, CuO/CeO_2-cube shows the worst performance for CO-PROX, mainly due to the weak interaction between copper oxide particles and the exposed [100] facet of nanocube-ceria.

1. Introduction

Polymer electrolyte membrane fuel cells (PEMFCs) can effectively convert the chemical energy of hydrogen into electricity without any emission of air pollutants at low operating temperature, which presents great potential as a substitute for conventional combustion engines in future mobile applications. Hydrogen is usually generated by steam reforming of hydrocarbons or bioethanol in combination with low-temperature water-gas shift (WGS) reaction, however, the products require a further purification treatment in order to avoid the small amount of CO to poison Pt anode of PEMFC. Among different possible purification methods, selective oxidation of CO with introduction of little oxygen in the excess hydrogen gas (CO-PROX) has been regarded as the most economic and efficient approach. In the numerous catalysts applied for CO-PROX, $CuO\text{-}CeO_2$ catalysts have shown promising catalytic performance, which could substitute noble metal catalysts (Au, Pt, Ru) [1-3], not only considering catalytic performance but also from an economical point of view. The performance of $CuO\text{-}CeO_2$ based catalysts in CO-PROX appears to be related to the competitive oxidation reactions between CO and H_2 [4-6]. The active sites for the oxidation of both CO and H_2 are generated by the copper oxide reduction process, which is correlated with an induction step taking place upon the interaction between copper and ceria [4, 7]. Therefore, the interfacial characteristics must in principle strongly affect the catalytic activity over these active sites.

Changing the geometric type of interacting surfaces is considered to be a possible way to tune interfacial interactions between the two oxide components. For example, Sujie Chang et al. found that Ag/CeO_2 catalysts with CeO_2-nanocubes (exposing [100] planes) and CeO_2-nanorods (mainly exposing [110] and [100] planes) supports could form different kinds and amount of Ag species as well as the concentrations and structures of oxygen vacancies in CO oxidation [8]. Fine Ag nanoparticles generated in Ag/CeO_2-nanocubes and Ag_n^+ clusters dominated in Ag/CeO_2-nanorods, while the former is much more capable of creating oxygen vacancies in CeO_2 than the latter. In a similar sense, Liu et al. reported that NO reduction by CO was demonstrated to be most favorable by CuO entities in contact with ceria-nanorods compared with ceria-nanocubes or nanopolyhedra (exposing [111] planes) [9]. Very recently, Guangquan Yi et al. evaluated the Au/CeO_2 catalysts with nanoscale CeO_2 of rods, cubes and polyhedral for CO-PROX in a hydrogen-rich gas and found that a strong effect of CeO_2 morphology is followed in the order: rods > polyhedra > cubes [10]. The Au/CeO_2-rods catalyst exhibits the lowest apparent activation energy comparing with the Au/CeO_2-polyhedra and Au/CeO_2-cubes. Similarly, Gamarra et al. also reported that CuO/CeO_2-rod and CuO/CeO_2-sphere (mainly exposing [111] planes) catalysts show similar catalytic activity for CO-PROX, which is obviously higher than that of CuO/CeO_2-cube [11]. However, in contrast to the above works, Han et al. found CuO/ceria-nanooctahedra (exposing [111] planes) possess higher CO oxidation activity than CuO/ceria-nanorods or nanocubes, probably due to the higher surface copper content on ceria-nanooctahedra than on ceria-nanorods or nanocubes [12].

Considering these apparent discrepancies and to gain a deeper understanding of the relationship between structure and catalytic performance for CuO/CeO_2 catalysts. In the present work, CuO/CeO_2 catalysts with different morphologies (rod, cube, plate and polyhedral) of ceria supports were prepared and the catalytic performance for CO selective oxidation in excess amounts of hydrogen (CO-PROX) was evaluated. TEM, XRD, BET, H_2-TPR, XPS, OSC mearument, UV-Raman and in-situ DRIFTS were employed to

[a] Institute of Catalysis, Zhejiang University, Hangzhou 310028, P.R. China. E-mail: zhourenxian@zju.edu.cn; Tel.: +86 571 88273290; Fax: +86 571 88273283.

characterize the structural property, redox property and the catalytic performance of the catalysts.

2. Experimental

2.1 Preparation of catalysts

Ceria-nanorod and ceria-nanocube were synthesized by modifying a previously reported recipe [13]. 4 mmol of $Ce(NO_3)_3{\cdot}6H_2O$ and 19.2 g of NaOH were dissolved in 10 and 70 mL of deionized water, respectively. The two solutions were mixed in a Teflon-lined autoclave and vigorously stirred for about 30 min. Then the autoclave was subjected to hydrothermal treatment at different temperatures (rods: 100 °C; cubes: 180 °C) for 24 h.

CeO_2-nanoplate was prepared by CTAB assisted hydrothermal synthesis method [14]. Briefly, 6 mmol of $Ce(NO_3)_3{\cdot}6H_2O$ and 2 mmol of CTAB were dissolved together in 80mL of deionized water in a Teflon bottle under stirring. Subsequently 8.0 mL $NH_3{\cdot}H_2O$ was added to the mixed solution, and then the mixture was transferred into a Teflon-lined autoclave. The autoclave was subjected to hydrothermal treatment at 100 °C for 24 h.

CeO_2-nanopolyhedra was synthesized as reported in literature[15], 8 mmol $Ce(NO_3)_3{\cdot}6H_2O$ was dissolved in 40 mL distilled water with magnetic stirring, followed by the addition of 1.0 g polyvinyl pyrrolidone (PVP, molecular weight = 3000 g/mol) under vigorous stirring for 20 min, forming a homogeneous solution. Next, 8mL $N_2H_4{\cdot}H_2O$ (85 %) was added dropwise to above solution under continuous stirring for 15 min. The mixed solution was transferred into a 100 mL Teflon-lined autoclave and subjected to hydrothermal treatment at 180 °C for 12 h.

After the hydrothermal treatment, the obtained four precipitates were separated by centrifugation, washed with deionized water and ethanol in turns, then dried at 80 °C overnight and calcined at 500 °C for 2 h. Samples of copper supported on the four CeO_2 supports (5.0 wt. % Cu) were prepared by incipient wetness impregnation with copper nitrate aqueous solutions. Then the samples were dried at 120 °C for 12 h, and calcined at 500 °C for 2 h in air. The catalysts were labeled as CuO/CeO_2-rod, CuO/CeO_2-cube, CuO/CeO_2-plate and CuO/CeO_2-polyhedra, respectively.

2.2. Catalytic performance tests

The activity measurement of the catalysts for selective oxidation of CO were carried out in a fixed-bed micro-reactor (quartz glass, i.d. = 6 mm) at atmospheric pressure. The mass of catalyst used in the tests was 100 mg which was crushed and sieved to 60-80 mesh and diluted with 100 mg inert α-alumina particles of the same mesh. The gas component was 50 % H_2, 1.0 % O_2, 1.0 % CO and Ar in balance to maintain the total flow rate as 100 mL min^{-1}, corresponding to a space velocity of 60,000 mL $g^{-1}h^{-1}$. Before activity measurements, the catalysts were pretreated in oxygen at 150 °C for 0.5 h.

The reactor outlet gases were measured by an on-line gas chromatograph which is outfitted with a flame ionization detector (FID) and a thermal conductivity detector (TCD) with Ar as carrier gas. CO and CO_2 were separated by a carbon molecular sieve (TDX-01) column, and converted to methane by a methanator and then detected by means of FID. The limit of FID detection for CO is less than 3 ppm. H_2 and O_2 were separated by 5A molecular sieve column and analyzed by means of TCD. In order to avoid the influence of CO_2 in the feed gas, we evaluate the CO conversion as follows:

$$\text{CO conversion} = \frac{[\text{CO}]_{in} - [\text{CO}]_{out}}{[\text{CO}]_{in}} \times 100(\%)$$

The O_2 selectivity was calculate from the oxygen mass balance as follows:

$$\text{O}_2 \text{ selectivity} = \frac{0.5([\text{CO}]_{in} - [\text{CO}]_{out})}{[\text{O}_2]_{in} - [\text{O}_2]_{out}} \times 100(\%)$$

2.3. Characterization of catalysts

Specific surface areas (S_{BET}) and BJH pore-size distribution of the catalysts were measured on Tristar II 3020 apparatus using N_2 adsorption isotherms at -195.8 °C, and the catalysts were out gassed at 250 °C under vacuum for 4 h. TEM image of the catalysts were obtained from a Hitachi-770 Transmission electron microscopy with resolution of 0.204nm. High resolution transmission electron microscopy (HR-TEM) images were obtained using a JEM-2100F apparatus operated at 200 kV. The sample was prepared by dipping a copper-grid supported transparent carbon foil in an ethanol solution, and the grid was dried in open air. X-ray powder diffraction patterns (XRD) were recorded on a Rigaku D/Max 2550 PC powder diffractometer with a Cu Kα radiation in the range of 20-80°. X-ray photoelectron spectra (XPS) were recorded on a PHI5000c spectrometer equipped with Al Kα radiation source (1486.6 eV) operating at 12.5 kV, and the calibration of the binding energy (BE) values is the C 1s peak at 284.8 eV. UV–Raman spectra were recorded on a UV-HR Raman spectrograph with a He-Gd laser of 325 nm excitation wavelength. The spectral resolution was 4 cm^{-1}, and the spectra acquisition consisted of 2 accumulations of 60 s for each sample.

The oxygen storage capacity complete (OSCC) measurement was carried out using a CHEMBET-3000 apparatus (Quantachrome Co.) equipped with TCD detector. The sample (100 mg) was first reduced under H_2 (10 ml/min) at 450 °C for 60 min, and then cooled down to 300 °C and flushed with He (30 ml/min) for 30 min. 0.25 ml of O_2 (high-purity, 99.999%) was pulsed into the sample bed every 5 min until no consumption of oxygen could be detected.

Temperature-programmed reduction (H_2-TPR) was carried out in a quartz fixed-bed micro-reactor. Before H_2-TPR measurement, 0.05 g of catalyst was pretreated in Ar flow at 300 °C for 0.5 h and cooled to room temperature. Then the sample was exposed to 5 vol % H_2/Ar with a flow rate of 40 mL min^{-1} and ramped from 40 to 700 °C (10 °C min^{-1}). The consumption of H_2 during the reduction process was measured by a thermal conductivity detector.

In situ diffuse reflectance infrared Fourier transform spectroscopy (DRIFTS) data was collected with a Nicolet 6700

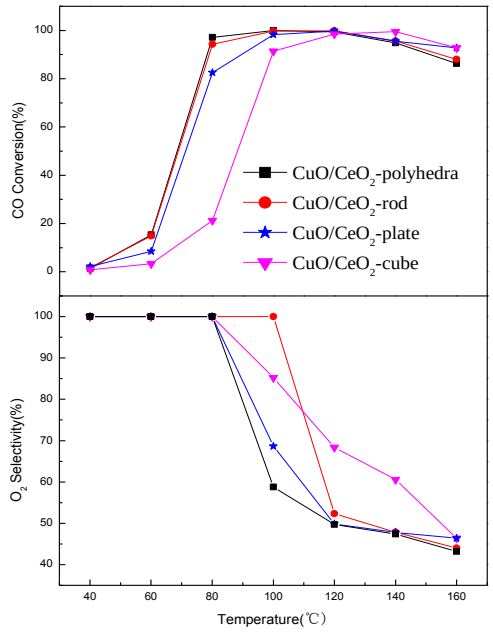

Fig. 1 The catalytic performance of CuO/CeO_2 catalysts with different morphologies.

apparatus equipped with an MCT detector. A diffuse reflection infrared cell, equipped with temperature controlled parts and CaF_2 window, was connected with a vacuum apparatus. Spectra were averaged over 32 scans with a resolution of 4 cm^{-1}. Prior to infrared experiment, the sample was pretreated with 10% O_2 at 300 °C for 0.5 h and then cooled to 25 °C in order to remove the contaminants from the catalyst surface. The composition of feed stream was 1 % CO, 1 % O_2, 50 % H_2 and Ar in balance. The deconvolution and integrated area of peaks was carried out by the Gaussian profiles.

3. Results and discussion

3.1 Catalytic performance of catalysts for CO-PROX reaction

Fig. 1 shows the catalytic performance of CuO/CeO_2 catalysts with different morphologies for the selective oxidation of CO in hydrogen-rich streams. The temperature of 50 % CO conversion (T_{50}) and the temperature window (CO conversion > 99.0 %) are listed in Table 1. According to T_{50}, CuO/CeO_2-rod and CuO/CeO_2-polyhedra obviously exhibit higher low-temperature oxidation activity for CO-PROX than CuO/CeO_2-plate and CuO/CeO_2-cube. Meanwhile, CuO/CeO_2-polyhedra shows the widest operating temperature window (about 45 °C, from 90 to 125 °C), which is only 30 °C (120-140 °C) for CuO/CeO_2-cube. When the reaction temperature elevates from 60 °C to 80 °C, CO conversion of CuO/CeO_2-polyhedra increases rapidly from 15.0 % to 95.0 % and keeps over 95.0 % at the temperature range of 80-150 °C.

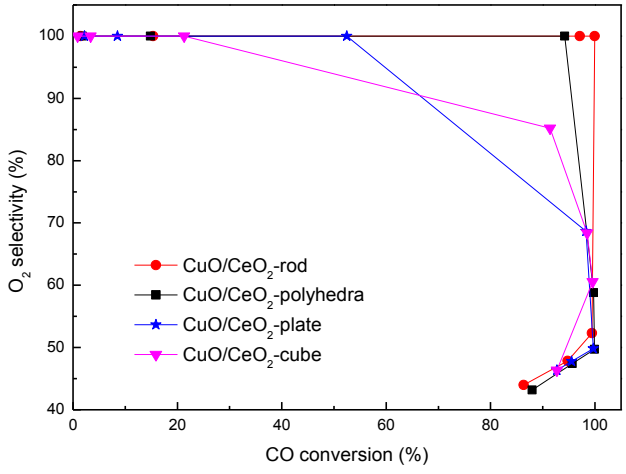

Fig. 2. O_2 selectivity for CO as a function of CO conversion.

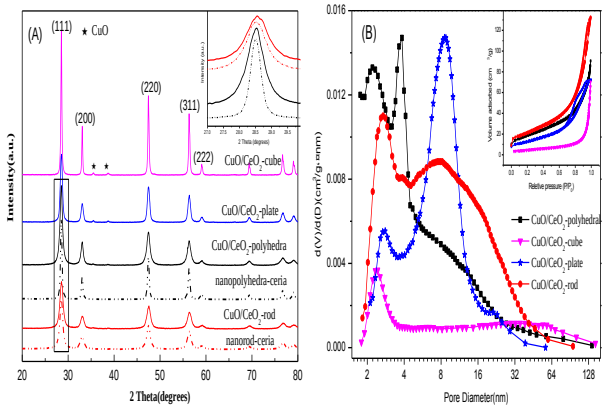

Fig. 3. XRD patterns (A) and BJH pore-size distribution curves combined with the N_2 adsorption/desorption isotherms (inset) (B) of CuO/CeO_2 catalysts with different morphologies.

As shown in Fig. 1, O_2 selectivity of CuO/CeO_2-rod keeps on 100 % from 40 to 100 °C which is much higher than the others. When the reaction temperature reaches to 120 °C, the competitive oxidation reaction between H_2 and CO occurs and the O_2 selectivity for CO steeply decreases. Fig. 2 intuitively shows the relationship between CO conversion and O_2 selectivity for CO of the four catalysts with different morphologies. We can see that CuO/CeO_2-rod and CuO/CeO_2-polyhedra shows relative higher catalytic performance than the other two no matter from the view pint of CO conversion or O_2 selectivity for CO.

3.2 Texture/structure properties of catalysts

XRD patterns of CuO/CeO_2 catalysts with different morphologies are exhibited in Fig. 3(A). All the catalysts show the characteristic peaks of fluorite-type oxide structure of CeO_2. However, two weak diffraction peaks of copper oxides in 35.6° and 38.7° are also observed over CuO/CeO_2-cube and CuO/CeO_2-plate, indicating more copper species aggregate on the CeO_2 supports, which could lead to the cover of surface active sites in the interface between copper and ceria and impair the catalytic activity of CuO/CeO_2 catalysts for CO-PROX. No extra peaks attributed to CuO are observed in XRD patterns of CuO/CeO_2-rod and CuO/CeO_2-polyhedra, indicating that CuO species are highly dispersed on the CeO_2 supports, which may be related to CeO_2 supports with higher surface area.

Table 1 lists the BET surface areas, crystallite size and lattice parameter of CuO/CeO_2 catalysts with different morphologies. Generally speaking, BET surface area is mainly determined by the

Table 1 Characteristics of CuO/CeO_2 catalysts and their activities in CO oxidation

Catalysts	S_{BET} (m^2/g)	Pore volume (cm^3/g)	CeO_2 lattice parameter (nm)	CeO_2 crystallite size (nm)	OSC (μmol O_2 /$g_{cat.}$)	T_{50} (°C)	Temperature window (°C)
CuO/CeO_2-rod	76.7	0.214	0.5405	9.9	524	68	95-125
CuO/CeO_2-cube	17.2	0.111	0.5413	56.6	368	89	120-140
CuO/CeO_2-plate	46.3	0.121	0.5411	17.0	477	71	100-120
CuO/CeO_2-polyhedra	67.1	0.147	0.5409	11.8	518	68	90-125

preparation procedures of materials. The specific surface areas of the catalysts are in this order: CuO/CeO_2-rod > CuO/CeO_2-polyhedra > CuO/CeO_2-plate >> CuO/CeO_2-cube. The S_{BET} is consistent with the crystallite size calculated from XRD results that CuO/CeO_2-rod and CuO/CeO_2-polyhedra show relative smaller partical size (about 10 nm) while that for CuO/CeO_2-cube (56.6 nm) is much bigger than the others. Based on S_{BET}, the surface copper atom density for the catalysts with different morphologies were calculated [16], which are 6.2, 7.1, 10.2 and 27.6 atoms/nm^2, respectively for CuO/CeO_2-rod, CuO/CeO_2-polyhedra, CuO/CeO_2-plate and CuO/CeO_2-cube. Lower surface density means better dispersion of copper oxide entities on the ceria support, which would decrease the aggregation of copper oxide to form crystalline phase CuO with large particle size and make for the catalytic activity of the catalyst. Thus large S_{BET} of CuO/CeO_2-rod and CuO/CeO_2-polyhedra is conducive to the distribution of CuO_x species, which is in favor of their catalytic performance for CO-PROX.

As listed in Table 1, CuO/CeO_2 catalysts with different morphologies possess different CeO_2 lattice parameters. For comparison, we also calculate the lattice parameters for bare CeO_2 with different morphologies. The lattice parameters are 0.5407, 0.5413, 0.5410 and 0.5412nm, respectively for nanorod-ceria, nanocube-ceria, nanoplate-ceria and nanopolyhedra-ceria. It is obviously that the impregnation of copper shrinks the lattice parameter of nanorod-ceria and nanopolyhedra-ceria to a certain degree, but the lattice parameters for nanocube-ceria and nanoplate-ceria have no change after the impregnation. Moreover, as shown in the inset view of Fig. 3(A), we can see that the characteristic peaks of nanorod-ceria and nanopolyhedra-ceria both shifts to higher angle after loading copper oxide, which is agreed with the reduced lattice parameter of CuO/CeO_2-rod and CuO/CeO_2-polyhedra catalysts. Due to the relative smaller radii of Cu^{2+} (0.073 nm) and Cu^{+} (0.077 nm) than Ce^{4+} (0.097 nm), we induce that a portion of copper ions substitute Ce^{4+} in the ceria lattice to increase the defect concentration in nanorod-ceria and nanopolyhedra-ceria, which improves their oxygen vacancy density and oxygen mobility, ultimately their catalytic performance for selective oxidation of CO in hydrogen-rich streams.

Fig. 3(B) shows BJH pore-size distribution curves and the N_2 adsorption/desorption isotherms of CuO/CeO_2 catalysts with different morphologies. The N_2 adsorption/desorption isotherms for the four catalysts corresponds to type IV along with an H3-type hysteresis loop without any limiting adsorption at high P/P_0, which is mainly due to the aggregates of platelike particles bring about slit-shaped pores [17]. Moreover, the existence of types H3 implies the irregular pore structure generating in the catalysts. Similarly, from Fig. 3(B), we can also get that the pore-size distribution for the CuO/CeO_2 catalysts is not uniform and the average pore size is large, indicating that the pores consist of the voids among original particles. All the CuO/CeO_2 catalysts possess porosity structures and the average pore diameters are 9.9, 22.8, 8.1 and 7.7 nm, respectively

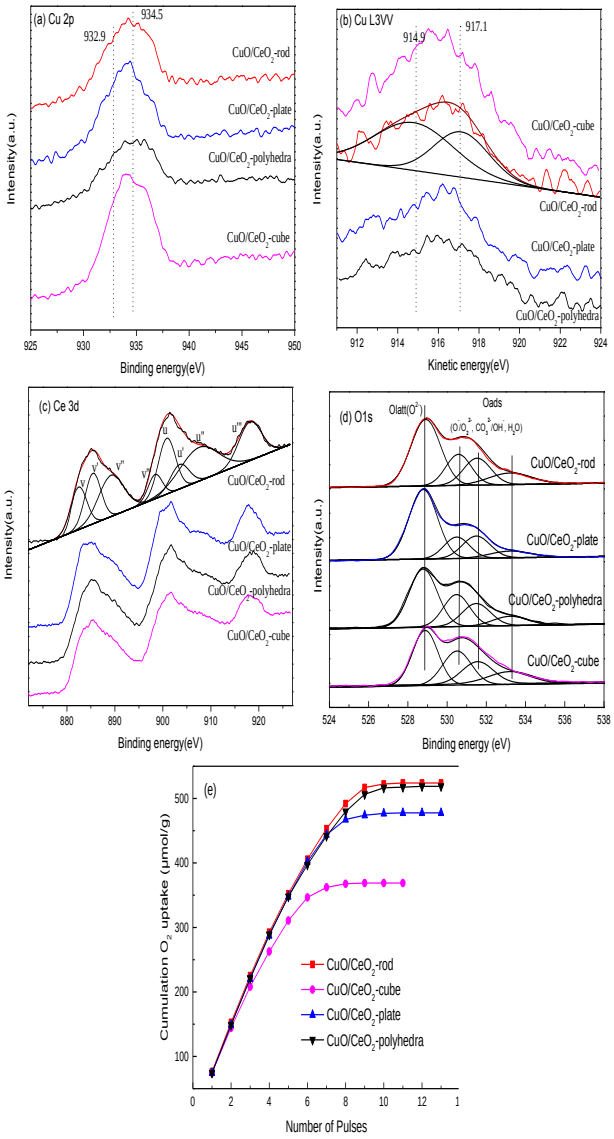

Fig. 4. XPS spectra (a-d) and OSC profile (e) of CuO/CeO_2 catalysts with different morphologies.

Table 2 Surface elemental composition and oxidation states of Ce/Cu in the CuO/CeO_2 catalysts with different morphologies by XPS analysis

Catalysts	Surface composition (at.%)				Cu/(Cu+Ce)	Cu^+ in Cu	Ce^{3+} in Ce	$O_{latt}/(O_{ads}+O_{latt})$
	Ce3d	Cu2p	O1s	C1s	(at.%)	(%)	(%)	(at.%)
CuO/CeO_2-rod	21.9	7.6	49.1	21.4	25.7	55.5	22.4	0.49
CuO/CeO_2-cube	17.7	9.5	50.6	21.2	30.0	43.3	15.7	0.39
CuO/CeO_2-plate	21.6	9.3	47.4	21.7	30.0	48.0	18.9	0.58
CuO/CeO_2-polyhedra	21.4	6.7	48.7	23.2	22.3	53.4	19.2	0.47

for CuO/CeO_2-rod, CuO/CeO_2-cube, CuO/CeO_2-plate and CuO/CeO_2-polyhedra. CuO/CeO_2-rod and CuO/CeO_2-plate catalysts mainly possess two kinds of mesoporous structures, from 2 to 4 nm and 4 to 64 nm, respectively. CuO/CeO_2-polyhedra possess more micropore besides mesoporous of 3-64 nm. However, the pore-size distribution for CuO/CeO_2-cube is the widest, maybe due to the relative bigger crystallite size. Meanwhile, an interesting observation is that the pore volumes of CuO/CeO_2-polyhedra and CuO/CeO_2-rod are 0.147 and 0.214 cm^3/g, respectively, which is significantly larger than others. The textural properties such as surface area, pore volume and average pore diameter, play an important role in the performance of catalytic carriers [18]. Comparing with the performance of the catalysts for CO-PROX, we deduce that larger surface area, smaller average pore size (<10 nm, such as 3 nm for CuO/CeO_2-rod, 2.5 nm and 4 nm for CuO/CeO_2-polyhedra) and narrow pore-size distribution are beneficial to the competitive catalytic reaction with high space velocity.

In order to obtain information of the surface elements distribution and the oxidation states of Ce/Cu, we analyzed XPS spectra of the Cu 2p, Cu L_3VV, Ce 3d and O 1s (Fig. 4), and listed the data about surface CuO_x/CeO_x and O species derived by XPS in Table 2. From Fig. 4(a), two characteristic peaks appear in the XPS spectra of Cu $2p_{3/2}$. The one centered at 934.5 eV is the characteristic peak of Cu^{2+}/CuO and the other one centered at 932.2-933.1 eV is regarded as the characteristic peak of Cu^+/Cu_2O [19, 20]. All the CuO/CeO_2 catalysts with different morphologies possess lower binding energy of Cu $2p_{3/2}$ (932.2-933.1 eV) and have no shake-up peak, which represents the existence of Cu^+ active sites in the catalysts. However, due to that the binding energy of Cu^+/Cu_2O is very close to that of Cu^{2+}/CuO, the XPS spectra of Cu $2p_{3/2}$ could not separate Cu^+/Cu_2O with Cu^{2+}/CuO distinctly. We further analyzed the kinetic energy spectra of the Auger L_3VV electron (Fig. 4(b)), in which the peaks centered at 917.1 eV and 914.9 eV are the characteristic peak of Cu^{2+} and Cu^+ respectively [19, 20]. From Table 2, it is obviously that the Cu contents of CuO/CeO_2-rod (25.7%) and CuO/CeO_2-polyhedra (22.3%) are much lower than the other two (30%), indicating more copper oxide penetrating into the surface lattice of nanorod-ceria and nanopolyhedral-ceria, which is accordant to the XRD result. Moreover, the relative content of Cu^+ is in the order: CuO/CeO_2-rod > CuO/CeO_2-polyhedra > CuO/CeO_2-plate > CuO/CeO_2-cube, which is basically consistent with their low-temperature catalytic activity. As shown in Fig. 5, we calculated the TOFs based on the mole of CO transformed per minute and per Cu at 60 °C, which are 0.084, 0.086, 0.048 and 0.018 min^{-1} respectively for CuO/CeO_2-rod, CuO/CeO_2-polyhedra, CuO/CeO_2-plate and CuO/CeO_2-cube. Along with the increase of the relative content of Cu^+, $T_{50\%}$ values of CuO/CeO_2 catalysts dramatically decrease and their TOF values increase. This result also implies that there is a stronger interaction between CuO_x species and rod/or polyhedra-ceria supports, which is beneficial to the stable existence of Cu^+ and the reduction from Cu^{2+} to Cu^+ on ceria surface, finally presenting great catalytic performance for CO-PROX.

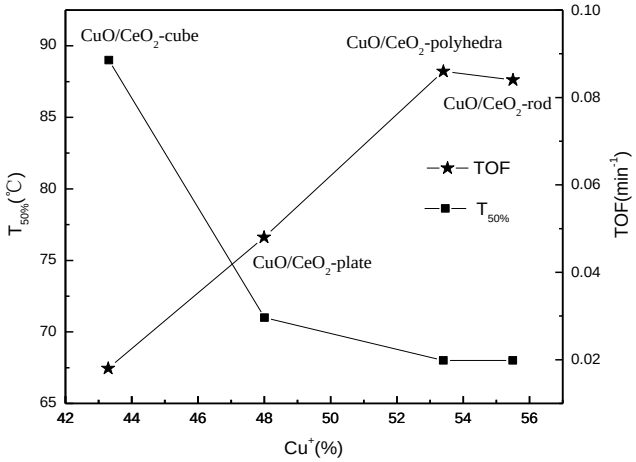

Fig. 5. TOF (60 °C)/$T_{50\%}$ values versus Cu^+ content for CuO/CeO_2 catalysts with different morphologies.

From Fig. 4(c), we can see that the Ce 3d spectrum curves consist of two series spin-orbit lines u and v. Ce $3d_{3/2}$ spin-obit components corresponding to the series of u mainly include three characteristic peaks labeled as u (900.6-901.0 eV), u" (907.5-907.7 eV) and u‴ (916.6-916.9 eV). Ce $3d_{5/2}$ spin-obit components corresponding to the series of v contain the three peaks of v (882.2-882.6 eV), v" (889.1-889.3 eV) and v‴ (898.2-898.5 eV). The above three pairs of peaks are attributed to the characteristic peaks of Ce^{4+}. Moreover, the residual two spectral lines labeled as u' (903.5-904.2 eV) and v' (885.1-885.8 eV) belong to the Ce^{3+} species. The proportion of Ce^{3+} ions with regard to the total cerium is calculated from the area ratio of the sum of the Ce^{3+} species to that of the total cerium species [21]. According to Table 2, CuO/CeO_2-rod and CuO/CeO_2-polyhedra have higher relative concentration of Ce^{3+} in Ce than CuO/CeO_2-cube and CuO/CeO_2-plate. The transform from Ce^{4+} to Ce^{3+} accompanying with the formation of oxygen vacancies is conductive for the adsorbed oxygen transferring to the reactive oxygen species and the lattice oxygen migrating from bulk to surface to participate in the redox reaction ($CO + O_{latt.} \rightarrow CO_2 + O_{vac}$; $O_2 + 2\ O_{vac} \rightarrow 2\ O_{latt.}$) [21, 22], thus the better catalytic performance of CuO/CeO_2-rod and CuO/CeO_2-polyhedra are very likely to be correlated with the higher amount of Ce^{3+}.

The XPS spectra of O 1s for CuO/CeO_2 catalysts with different morphologies are shown in Fig. 4(d) and the fitting peak information is listed in Table 2. There are two characteristic peaks occurring in the O 1s spectra of the four catalysts. The primary band (528.7-529.1eV) denoted as O_{latt} represents the characteristic of the lattice oxygen bound to CuO and CeO_2 phases, while the shoulder band (530.0-535.2 eV) is attributed to chemisorbed oxygen peak (O_{ads}) including adsorbed oxygen (O^-/O_2^{2-}), hydroxyl and carbonate species as well as adsorbed water [23]. Generally, O_{latt} is thought to be a key factor which participates into the rate-limiting step of the whole redox reaction for CO-PROX and much more O_{latt} species existing on the surface of the catalyst would promote the catalytic performance. However, the concentration of lattice oxygen ($O_{latt}/(O_{ads}+O_{latt})$ for the catalysts is in the order: CuO/CeO_2-plate > CuO/CeO_2-rod, CuO/CeO_2-polyhedra > CuO/CeO_2-cube, which is not accordant with the order of their catalytic activity. It indicates that the lattice oxygen may be not the decisive factor of the four catalysts for CO-PROX, whose catalytic performance could be influenced by multiple factors such as their texture and redox properties, the interfacial interaction between CuO_x and CeO_2 species, especially the concentration of Cu^+ species, etc.

Fig. 4(e) shows the cumulation O_2 uptake amount as a function of the number of pulses of the four CuO/CeO_2 catalysts with different morphologies. Obviously, OSC of the samples is in this order: CuO/CeO_2-rod (524 μmol/$g_{cat.}$) > CuO/CeO_2-polyhedra (518 μmol/$g_{cat.}$) > CuO/CeO_2-plate (477 μmol/$g_{cat.}$) > CuO/CeO_2-cube (368 μmol/$g_{cat.}$). The oxygen storage capacity is closely related to the presence of oxygen vacancies and the mobility of oxygen in ceria, which is important to obtain a highly active catalyst for CO oxidation. The higher OSC of CuO/CeO_2-rod and CuO/CeO_2-polyhedra combined with their higher amount of Ce^{3+} both indicate better oxygen mobility which promote the redox cycle between Ce^{3+}/Ce^{4+} and Cu^{2+}/Cu^+.

UV-Raman spectroscopies of the catalysts afford us the information about their oxygen lattice vibrations. Fig. 6 shows UV-Raman profiles (A) and TOF/$T_{50\%}$ values versus A_{584}/A_{454} ratio (B) of CuO/CeO_2 catalysts with different morphologies. Usually, the band at about 584 cm^{-1} can be linked to the oxygen vacancies in the CeO_2 lattice and attributed to the presence of defective structure in CeO_2 [21]. Based on the viewpoint in literature [24], the area ratio (A_{584}/A_{454}) of the peaks between 584 cm^{-1} and 454 cm^{-1} can represent the relative concentration of oxygen vacancies. CuO/CeO_2-rod shows a much higher A_{584}/A_{454} ratio (1.22) and CuO/CeO_2-polyhedra is second (1.10), while the A_{584}/A_{454} ratios for CuO/CeO_2-plate and CuO/CeO_2-cube are only 75% of that for CuO/CeO_2-rod. This suggests that CuO/CeO_2-rod and CuO/CeO_2-polyhedra catalysts possess more oxygen vacancies compared with other catalysts, which is in consistence with the result of XPS. The more oxygen vacancies not only favor the stable existence of Cu^+ species, but also promote the diffusion of the surface adsorbed oxygen on the catalysts [25], and further increase the CO oxidation catalytic activity of the catalysts. As shown Fig. 6(b), it can be clearly seen that bigger value of A_{584}/A_{454} matches to lower $T_{50\%}$ and higher TOFs, that is to say, better catalytic performance.

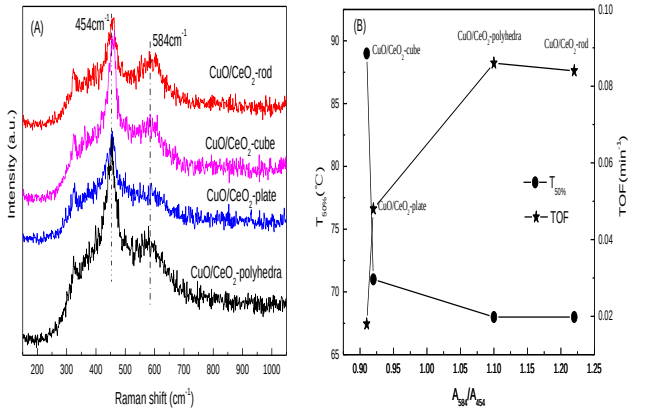

Fig. 6. UV-Raman profiles (a) and TOF (60 °C)/$T_{50\%}$ values versus A_{584}/A_{462} ratio (b) of CuO/CeO_2 catalysts with different morphologies.

3.3 Morphologies of catalysts

According to TEM images in Fig. 7, CuO/CeO_2 catalysts with different morphologies were successfully prepared. It can be obtained that CuO/CeO_2-rod catalyst is short rod-like nanoparticle with a diameter of about 5 nm and lengths varying from 15 to 30 nm. CuO/CeO_2-plate is rhombic or hexagonal plate with a diameter of 10 nm and a thickness of ~ 4 nm. CuO/CeO_2-polyhedra is irregular polygon particles with a diameter of 5-10 nm. CuO/CeO_2-cube is non uniform cube block with a diameter of 20-60 nm and has bigger particle size compared to other samples, basically consistent with the XRD results (Table 1). Generally, the exposed crystal face takes an

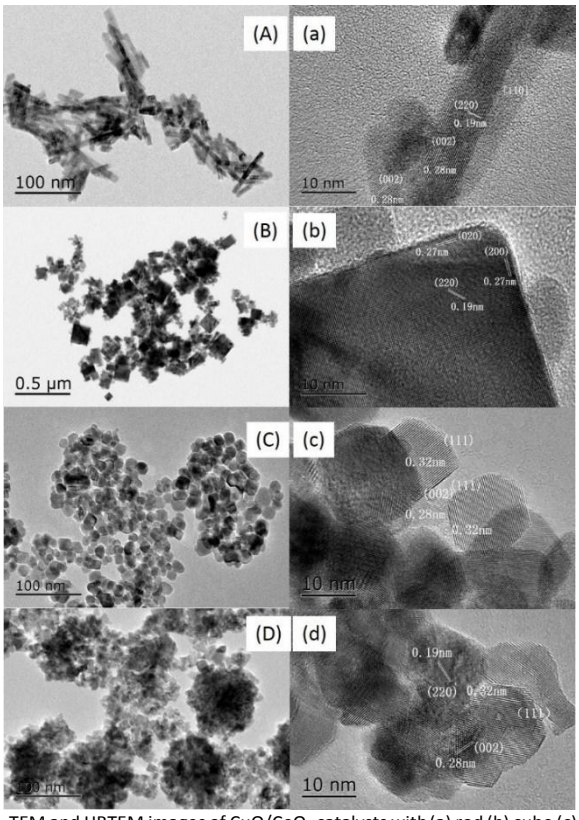

Fig. 7. TEM and HRTEM images of CuO/CeO_2 catalysts with (a) rod (b) cube (c) plate (d) polyhedral morphologies.

Table 3 peak temperature and peak area of H_2-TPR peaks for CuO/CeO_2 catalysts

Catalysts	α Peak		β Peak		γ Peak		Total H_2 cons ($\mu mol/g_{cat}$)
	Peak temp. (°C)	H_2 cons ($\mu mol/g_{cat}$)	Peak temp. (°C)	H_2 cons ($\mu mol/g_{cat}$)	Peak temp. (°C)	H_2 cons ($\mu mol/g_{cat}$)	
CuO/CeO_2-rod	141	270	164	336	176	240	846
CuO/CeO_2-cube	144	76	161	294	183	346	716
CuO/CeO_2-plate	144	178	163	218	176	452	848
CuO/CeO_2-polyhedra	144	282	164	472	187	195	949

*Theoretical H_2 consumption of CuO/CeO_2 catalysts with 5.0 wt. % Cu is 787$\mu mol/g_{cat}$.

important role in the catalytic performance of the catalysts. Due to the lower surface energy, [111] planes is much more stable than [110] and [001] plans thus not active than the later. The nanorod-ceria mainly exposes [110] and [001] planes, nanocube-ceria exposes [100] plane, nanoplate-ceria is dominated by [111] plane, and nanopolyhedra-ceria is enclosed by the [111] and [100] facets. Previous researches [26] found that when gold was deposited on rod, cubic, or polyhedral shapes of ceria, the Au/ceria-rods had the best activity for the water-gas shift reaction at 150-350 °C. They insisted that the high CO conversion is due to the smallest oxygen vacancy formation energy of [110] planes for ceria-rods which is in favor of anchoring and dispersing very fine gold clusters. However, the above analyses of XPS indicate that nanopolyhedra-ceria mainly exposing [111] and [100] plane also interacts strongly with CuO species and there exists much Cu^+ species in CuO/CeO_2-polyhedra, facilitating the CO oxidation activity at low temperature range to a great degree. The following results about H_2-TPR and in situ DRIFTS also further evidence this interesting finding.

3.4 Redox properties of catalysts

As is well-known, the reduction properties of supported metal oxide catalysts may be changed due to the interaction between metal and support. The H_2-TPR profiles for bare CeO_2 and CuO/CeO_2 catalysts with different morphologies are shown in Fig. 8 and the peak temperature and H_2 consumption of H_2-TPR peaks are listed in Table 3. For bare CeO_2 samples, the peaks below 600 °C can be attributed to the reduction of surface oxygen, subsurface oxygen and surface Ce^{4+} species [27, 28]. The reduction temperature of nanorod-ceria is the lowest and it shows large amount of H_2 consumption, while the reduction behaviour of nanocube-ceria is opposite to nanorod-ceria, which may be related with less BET surface area and bigger particle size compared to that of other samples. For CuO/CeO_2 catalysts, three reduction peaks appear in its TPR profile at about 145 °C (peak α), 160 °C (peak β) and 190 °C (peak γ), respectively. The peak α is ascribed to the reduction of the highly dispersed CuO_x species strongly interacting with the ceria. And the peak β is ascribed to the reduction of CuO_x species weakly interacting with ceria [29]. The peak γ is attributed to the reduction of a mixture of crystalline CuO and Cu^+ due to that the reduction temperature of Cu^+ stably existing in the oxygen vacancies is relatively higher than CuO_x species weakly interacting with ceria and much close to crystalline CuO [30]. From Table 3, it can be seen that the H_2 consumption of peak α is in the order: CuO/CeO_2-polyhedra > CuO/CeO_2-rod > CuO/CeO_2-plate > CuO/CeO_2-cube, which is in agreement with the catalytic activity change of catalysts for CO-PROX. It indicates that more copper species strongly interacting with ceria would enhance the interfacial interaction between copper and ceria and increase the catalytic activity for CO-PROX. However, many studies [5, 31] also show that Cu^+ species are the main adsorptive and active centers of CO oxidation. Due to XRD result, there is no crystalline CuO appearing in CuO/CeO_2-polyhedra and CuO/CeO_2-rod, their H_2 consumption of peak γ are mainly caused by the reduction of Cu^+ species while the other two catalysts show two distinctive diffraction peaks of copper oxides in their XRD patterns which is the other reason for the appearance of peak γ. In addition, as shown in Table 3, the total H_2 consumptions of CuO/CeO_2-rod, CuO/CeO_2-polyhedra and CuO/CeO_2-plate are much higher than the theoretical H_2 consumption of CuO/CeO_2 catalysts with 5.0 wt. % Cu (787$\mu mol/g_{cat}$). This indicates that hydrogen spillover occurs to these three catalysts and a portion of Ce^{4+} were reduced to Ce^{3+} causing the formation of oxygen vacancies in them. Higher content of oxygen vacancies in the catalysts is benefit to improving the catalytic performance. Thus, the hydrogen spillover may be another reason for the better catalytic activities of CuO/CeO_2-polyhedra and CuO/CeO_2-rod in CO-PROX. On the other hand, it is found that the total hydrogen consumption of CuO/CeO_2-cube is lower than the theoretical for CuO reduction. The main reason for this behavior is due to the existence of Cu^+ and weak or none interaction between copper and ceria support in CuO/CeO_2-cube. As is revealed by XPS results (Table 2), a portion of Cu^+ can be found on the surface of the four catalysts and it is obvious that the

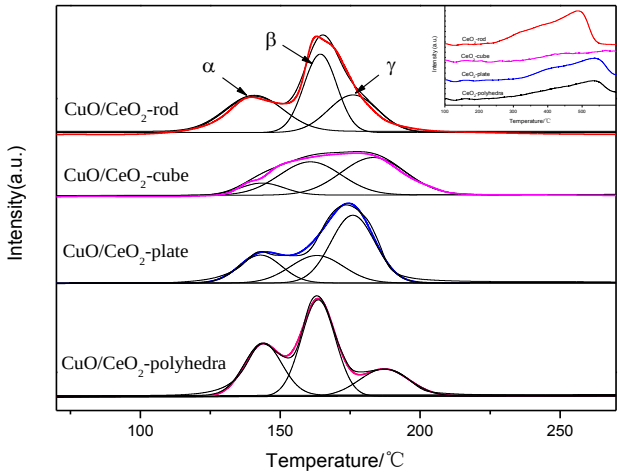

Fig. 8. H_2-TPR profiles of CuO/CeO_2 catalysts with different morphologies.

H_2 consumption of Cu^+ is much less than CuO, while the theoretical H_2 consumption of CuO/CeO_2 catalyst was calculated based on the complete reduction of CuO. On the other hand, the weak or none interaction between copper and ceria support in CuO/CeO_2-cube could not lead to the reduction of Ce^{4+} to Ce^{3+} on the ceria support. Therefore, the total hydrogen consumption of CuO/CeO_2-cube is lower than the theoretical for CuO reduction. As for the other three catalysts, the reduction of Ce^{4+} to Ce^{3+} caused by the relative strong interaction between copper and ceria makes their total H_2 consumption much higher than the theoretical H_2 consumption of CuO/CeO_2 catalysts.

3.5 In situ-DRIFTS

In order to test the potential relationship between the active species and catalytic behavior during CO-PROX, in situ DRIFTS studies under reaction system were performed. Fig. 9 present DRIFTS spectra recorded under CO + O_2 + H_2 reaction stream over CuO/CeO_2 catalysts with different morphologies. The DRIFTS spectra are subdivided into three characteristic zones of wavenumber. Specifically, bands in the highest wavenumber zone (3800-2650 cm^{-1}) correspond mainly to hydroxyl species, including isolated hydroxyls and associated species [32, 33]. The bands below 1750 cm^{-1} are attributed to carbonate, carboxylate or formate species [34]. These spectra over CuO/CeO_2 catalysts have no significant difference with each other, thus, are not showed in this paper. The zone in 2400-2000 cm^{-1} is mainly composed of the vibrations of two species, CO_2 (g) and Cu^{n+}-CO species. The generation of CO_2 (g) can be represented by the rotational vibration at 2359 and 2339 cm^{-1}, which is usually correlated with the catalytic activity of CO oxidation [35].

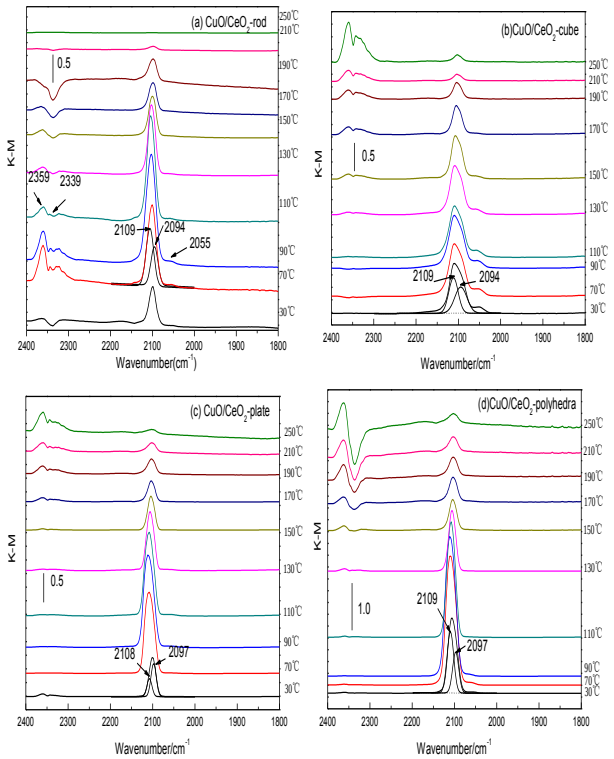

Fig. 9. DRIFTS spectra of CuO/CeO_2 catalysts with different morphology recorded under the simple CO+O_2+H_2 reaction stream.

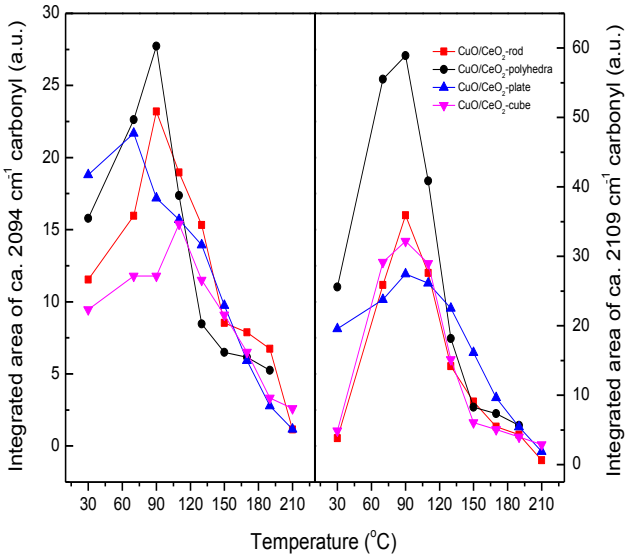

Fig. 10. Intensity of Cu^+- carbonyls as a function of reaction temperature under the indicated CO + O_2 + H_2 reaction mixtures.

Multiple bands assigned to a spontaneous variation of carbonyl species appear in the range of 2200-2000 cm^{-1}. According to previous findings [34-39], the vibrations for the Cu^{n+}-CO species, such as CO adsorption on Cu^{2+}, Cu^+ and Cu^0 sites, typically focus on the regions of 2200-2140 cm^{-1}, 2140-2100 cm^{-1} and 2100-2000 cm^{-1}, respectively. Usually, the band at 2065 cm^{-1} represents CO adsorption at small metallic copper clusters as well as Cu^{2+}-CO species is unstable and could not exist at room temperature. As shown in Fig. 9, only bands that assigned to Cu^+-CO species in the regions of 2200 - 2000 cm^{-1} are observed over all the CuO/CeO_2 catalysts, except for CuO/CeO_2-cube, in which band assigned to Cu^0-CO species is also observed at about 2050 cm^{-1}. The bands at 2140-2100 cm^{-1} are considered to be the most informative region because it reflects the adsorption of CO at Cu^+ sites, which is the active center of the redox reaction [5, 31, 34, 35]. The intensity of bands corresponding to Cu^+-CO species over CuO/CeO_2-polyhedra and CuO/CeO_2-rod is obviously higher than that of CuO/CeO_2-plate and CuO/CeO_2-cube, indicating that the former possess more Cu^+ species, which is in good agreement with the results of above XPS and H_2-TPR. Actually, the band in the regions of 2140-2100 cm^{-1} can be subdivided into two characteristic zones of wavenumber, which represents two kinds of copper species that possess different interaction strength with ceria support. The low-frequency of Cu^+-CO at 2094 cm^{-1} is attributed to the smaller copper oxide clusters subjected to a strong interaction with ceria due to the presence of a stronger M-C bond and a weaker C-O bond, which justifies the relatively strong red shift produced in the Cu^+-carbonyl stretching. In contrast, the high-frequency of Cu^+-CO at 2109 cm^{-1} belongs to the copper oxide clusters with bigger size interacting weakly with ceria [5].

For CuO/CeO_2-polyhedra catalyst, the intensity of the bands at 2109 cm^{-1} and 2094 cm^{-1} is the largest at the low temperature range and first increases and then reaches a maximum at 90 °C, which maybe involve with the reducing of the partial Cu^{2+} and the formation of more Cu^+ species. With further increasing the reaction temperature, the two peaks are weakened. The same phenomenon

occurs on other CuO/CeO_2 catalysts with different morphology. According to the literature [5], the intensity of the two bands is responsible for the CO oxidation activity of the catalysts. In order to further clarify the contribution of the two Cu^+-carbonyls to CO oxidation activity for CO-PROX in H_2-rich streams, correlation of the intensity of two Cu^+-carbonyls versus the reaction temperature is exhibited in Fig. 10. The intensity of band at 2094 cm^{-1} follows the order: CuO/CeO_2-polyhedra > CuO/CeO_2-rod > CuO/CeO_2-plate > CuO/CeO_2-cube, while that of band at 2109 cm^{-1} is CuO/CeO_2-polyhedra > CuO/CeO_2-rod > CuO/CeO_2-cube > CuO/CeO_2-plate.

Obviously, the variation of the intensity of band at 2094 cm^{-1} is basically consistent with that of catalytic activity, indicating that more copper oxide cluster with strong interaction with ceria, including in Cu^+ and highly dispersed CuO species, apparently promote the catalytic activity of the catalyst for CO-PROX. However, for CuO/CeO_2-cube, it shows lower intensity at 2094 cm^{-1}. Moreover, Cu^0-CO species appears at about 2050 cm^{-1}, indicating that there is more copper species with bigger particle size interacting weakly with ceria. Thus we infer that it may be the most important reason for the poor catalytic performance of CuO/CeO_2-cube.

4. Conclusion

We studied morphologies effect of ceria (rod, cube, plate and polyhedral) on CuO/CeO_2 catalysts synthesized by impregnation method for CO selective oxidation in excess amounts of hydrogen (CO-PROX). TEM, XRD, BET, OSC, H_2-TPR, XPS, and DRIFTS were employed to characterize the structure, redox property and the catalytic performance of the catalysts. The catalytic performance tests show that CuO/CeO_2-rod and CuO/CeO_2-polyhedra exhibit higher low-temperature catalytic oxidation activity coupled with broader operating temperature "window" (CO conversion > 99.0 %, 95-125 °C and 90-125 °C, respectively) in CO selective oxidation reaction. CuO/CeO_2-rod and CuO/CeO_2-polyhedra both possess higher content of the active spices Cu^+, the smaller copper oxide clusters subjected to a strong interaction with ceria and more oxygen vacancies on the surface of the catalysts, which may be one of the main reasons for its higher catalytic activity of CO oxidation than other catalysts. In addition, higher specific surface area, smaller average pore size and concentrated pore-size distribution of mesopores are also beneficial to improve the catalytic performance.

Acknowledgements

We gratefully acknowledge the financial supports from Nature Science Foundation of China (No. 21477109).

Notes and references

1 W.B. Kim, T. Voitl, G.J. Rodriguez-Rivera, S.T. Evans and J.A. Dumesic, *Angew. Chem. Int. Ed.*, 2005, **44**, 778-782.
2 C. Rossignol, S. Arrii, F. Morfin, L. Piccolo, V. Caps and J.L. Rousset, *J. Catal.*, 2005, **230**, 476-483.
3 S. Alayoglu, A.U. Nilekar, M. Mavrikakis and B. Eichhorn, *Nat. Mater.*, 2008, **7**, 333-338.
4 D. Gamarra, G. Munuera, A.B. Hungría, M. Fernández-García, J.C. Conesa, P.A. Midgley, X.Q. Wang, J.C. Hanson, J.A. Rodríguez and A. Martínez-Arias., *J. Phys. Chem. C*, 2007, **111**, 11026-11038.
5 D. Gamarra, C. Belver, M. Fernández-García and A. Martínez-Arias., *J. Am. Chem. Soc.*, 2007, **129**, 12064-12065.
6 H.C. Lee, D.H. Kim, *Catal. Today*, 2008, **132**, 109-116.
7 A. Martínez-Arias, A.B. Hungría, M. Fernández-García, A. Iglesias-Juez, J. Soria, J.C. Conesa, J.A. Anderson and G. Munuera, *Phys. Chem. Chem. Phys.*, 2012, **14**, 2144-2151.
8 S. Chang, M. Q. Hua, L. Zhang, Y. Ma, B. Ye and W. Huang, *J. Catal.*, 2012, **293**, 195-204.
9 L. Liu, Z. Yao, Y. Deng, F. Gao, B. Liu and L. Dong, *ChemCatChem*, 2011, **3**, 978-989.
10 G. Yi, H. Yang, B. Li, H. Lin, K. Tanakab and Y. Yuan, *Catal. Today*, 2010, **157**, 83-88.
11 D. Gamarra, A. Lopez Camara, M. Monte, S.B. Rasmussen, L.E. Chinchilla, A.B. Hungria, G. Munuera, N. Gyorffy, Z. Schay, V. Cortes Corberan, J.C. Conesa and A. Martinez-Arias, *Appl. Catal., B*, 2013, **130-131**, 224-238.
12 Jaeman Han, Hyung Jun Kim, Sangwoon Yoon and Hyunjoo Lee, *J. Mol. Catal., A*, 2011, **335**, 82-88.
13 H. Mai, L. Sun, Y. Zhang, R. Si, W. Feng, H. Zhang, H. Liu and C. Yan, *J. Phys. Chem., B*, 2005, **109**, 24380-24385.
14 C. Pan, D. Zhang and L. Shi, *J. Solid State Chem.*, 2008, **181**, 1298-1306.
15 F. Lu, F. Meng, L. Wang, J. Luo and Y. Sang, *Mater. Lett.*, 2012, **73**, 154-156.
16 M. Monte, D. Gamarra, A. López Cámara, S.B. Rasmussen, N. Gyorffy, Z. Schay, A. Martínez-Arias and J.C. Conesa, *Catal. Today*, 2014, **229**, 104-113.
17 K.S.W. Sing, D.H. Everett, R.A.W. Haul, L. Moscou, R.A. Pierotti, J. Rouquérol and T. Siemieniewska, *Pure Appl. Chem.*, 1985, **57**, 603-619.
18 Z.L. Wei, H.M. Li, X.Y. Zhang, S.H. Yan, Z. Lv, Y.Q. Chen and M.C. Gong, *J. Alloys Compd.*, 2008, **455**, 322-326.
19 Y.Z. Chen, B.J. Liaw, W.C. Chang and C.T. Huang, *Int. J. Hydrogen Energy*, 2007, **32**, 4550-4558.
20 Y.Z. Chen, B.J. Liaw and H.C. Chen, *Int. J. Hydrogen Energy*, 2006, **31**, 427-435.
21 J. Fan, X. Wu, X. Wu, Q. Liang, R. Ran and D. Weng, *Appl. Catal., B*, 2008, **81** 38-48.
22 P. Dutta, S. Pal, M.S. Seehra, Y. Shi, E.M. Eyring and R.D. Ernst, *Chem. Mater.*, 2006, **18**, 5144-5146.
23 K. Sutthiumporn and S. Kawi, *Int. J. Hydrogen Energy*, 2011, **36**, 14435-14446.
24 Q. Liang, X. Wu, D.Weng and H. Xu, *Catal. Today*, 2008, **39**, 113-118.
25 J. Chen, Y. Zhan, J. Zhu, C. Chen, X. Lin and Q. Zheng, *Appl. Catal., A*, 2010, **377**, 121-127.
26 R. Si and M. Flytzani-Stephanopoulos, *Angew. Chem. Int. Ed.*, 2008, **47**, 2884-2887.
27 X. Tang, Y. Li, X. Huang, Y. Xu, H. Zhu, J. Wang and W. Shen, *Appl. Catal., B*, 2006, **62**, 265-273.
28 A. Trovarelli, *Catal. Rev. Sci. Eng.*, 1996, **38**, 439-520.
29 S. P. Wang, T. Y. Zhang, Y. Su, S. R. Wang, S. M. Zhang, B. L. Zhu and S. H. Wu, *Catal. Lett.*, 2008, **121**, 70-76.
30 J. Li, P.F. Zhu and R.X. Zhou, *J. Power Sources*, 2011, **196**, 9590-9598.
31 P. Bera, A.L. Camara, A. Hornes and A. Martinez-Arias, *J. Phys. Chem., C*, 2009, **113**, 10689-10695.
32 A. Badri, C. Binet and J.-C. Lavalley, *J. Chem. Soc. Faraday Trans.*, 1996, **92**, 4669-4673.
33 C. Binet, M. Daturi and J.-C. Lavalley, *Catal. Today*, 1999, **50**, 207-225.
34 A. Hornes, P. Bera, A.L. Camara, D. Gamarra, G. Munuera and A. Martinez-Arias, *J. Catal.*, 2009, **268**, 367-375.
35 D. Gamarra and A. Martinez-Arias, *J. Catal.*, 2009, **263**, 189-195.
36 M. Manzoli, R.D. Monte, F. Boccuzzi, S. Coluccia and J. Kaˇspar, *Appl. Catal., B*, 2005, **61**, 192-205.

37 F. Boccuzzi, G. Ghiotti and A. Chiorino, *Surf. Sci.*, 1985, **162**, 361-367.
38 R. Kydd, D. Ferri, P. Hug, J. Scott, W.Y. Teoh and R. Ama, *J. Catal.*, 2011, **277**, 64-71.
39 D. Scarano, S. Bordiga, C. Lamberti, G. Spoto, G. Ricchiardi, A. Zecchina and C. Otero Arean, *Surf. Sci.*, 1998, **411**, 272-285.

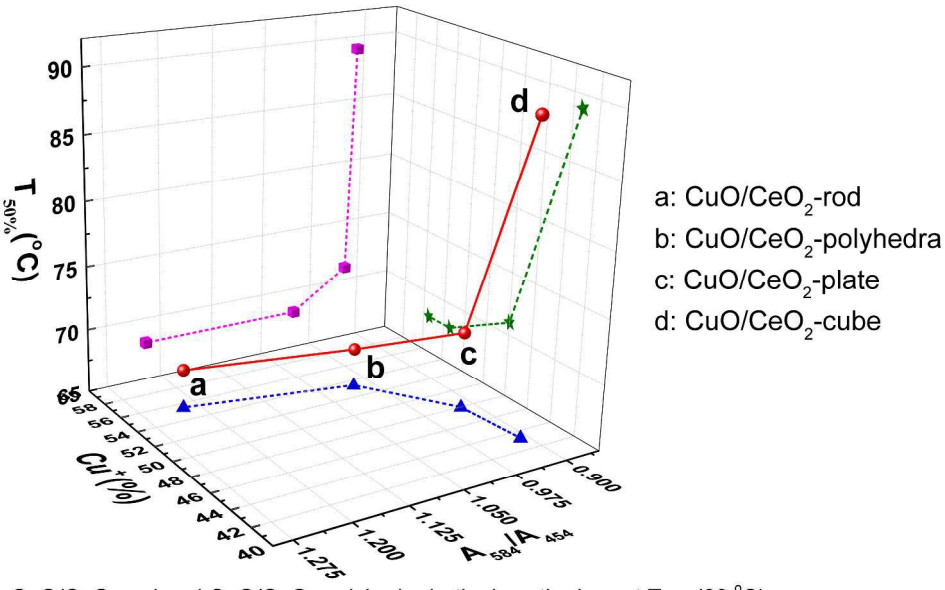

CuO/CeO_2-rod and CuO/CeO_2-polyhedra both show the lowest $T_{50\%}$ (68 °C) for CO-PROX, due to higher content of Cu^+ and oxygen vacancies.

285x196mm (300 x 300 DPI)